BNL-205685-2018-JAAM

Advances in X-ray optics: From metrology characterization to wavefront sensing-based optimization of active optics

D. Cocco, M. Idir

To be published in "Nuclear Instruments And Methods in Physics Research, A"

March 2018

Photon Sciences

Brookhaven National Laboratory

U.S. Department of Energy

USDOE Office of Science (SC), Basic Energy Sciences (BES) (SC-22)

Notice: This manuscript has been authored by employees of Brookhaven Science Associates, LLC under Contract No. DE-SC0012704 with the U.S. Department of Energy. The publisher by accepting the manuscript for publication acknowledges that the United States Government retains a non-exclusive, paid-up, irrevocable, world-wide license to publish or reproduce the published form of this manuscript, or allow others to do so, for United States Government purposes.

DISCLAIMER

This report was prepared as an account of work sponsored by an agency of the United States Government. Neither the United States Government nor any agency thereof, nor any of their employees, nor any of their contractors, subcontractors, or their employees, makes any warranty, express or implied, or assumes any legal liability or responsibility for the accuracy, completeness, or any third party's use or the results of such use of any information, apparatus, product, or process disclosed, or represents that its use would not infringe privately owned rights. Reference herein to any specific commercial product, process, or service by trade name, trademark, manufacturer, or otherwise, does not necessarily constitute or imply its endorsement, recommendation, or favoring by the United States Government or any agency thereof or its contractors or subcontractors. The views and opinions of authors expressed herein do not necessarily state or reflect those of the United States Government or any agency thereof.

Advances in X-ray optics: From metrology characterization to wavefront sensing-based optimization of active optics

Daniele Cocco [a], Mourad Idir [b], Daniel Morton [a], Lorenzo Raimondi [c], Marco Zangrando [c,d,*]

[a] SLAC National Accelerator Laboratory, 2575 Sand Hill Rd., Menlo Park, CA, 94025, United States
[b] Brookhaven National Laboratory - NSLS II, 50 Rutherford Dr. Upton, NY, 11973, United States
[c] Elettra—Sincrotrone Trieste SCpa, S.S. 14 km 163.5 in Area Science Park, 34149 Trieste, Italy
[d] IOM-CNR, S.S. 14 km 163.5 in Area Science Park, 34149 Trieste, Italy

ABSTRACT

Experiments using high brightness X-rays are on the forefront of science due to the vast variety of knowledge they can provide. New Synchrotron Radiation (SR) and Free Electron Laser (FEL) light sources provide unique tools for advanced studies using X-rays. Top-level scientists from around the world are attracted to these beamlines to perform unprecedented experiments. High brightness, low emittance light sources allow beamline scientists the possibility to dream up cutting-edge experimental stations. X-ray optics play a key role in bringing the beam from the source to the experimental stations.

This article explores the recent developments in X-ray optics. It touches on simulations, diagnostics, metrology and adaptive optics, giving an overview of the role X-ray optics have played in the recent past. It will also touch on future developments for one of the most active field in the X-ray science.

0. Introduction

One of the key developments that has pushed Synchrotron Radiation (SR) and Free Electron Laser (FEL) science is the ability to manipulate the photon beam, preserve the source quality, and adapt the X-ray beam to the needs of the experiments. Often taken for granted by the beamline scientists, X-ray optics played a major role in making the 2nd and 3rd generation SR sources and FELs useful for X-ray experiments like microscopy, inelastic scattering, high resolution photoelectron spectroscopy, diffraction experiments and many more.

The development of new optics, dispersive and diffractive elements, coatings, cooling schemes, simulation tools and new methods of beam characterization, is usually fostered in small laboratories or by small groups and then adopted by the entire community. Some of the noteworthy developments that have had major impacts in this field include: Zone Plates, which have seen higher and higher spatial resolution [1,2] and, more recently, higher and higher aspect ratio [3]; the Long Trace Profiler [4] which boosted metrology and impacted mirror quality in the nineties; the multilayer deposition techniques, recently used for nano-focusing applications [5]; crystal monochromators. With the advent of the 3rd generation light source, many facilities recognized the need to invest human capital in the development of tools for X-ray optics and for optimizing the performance of the beamlines. This effort produced new optical designs, with higher resolution, higher flux and overall better performances. The once feared variable line space grating is

now commonly used, producing more flexible and compact optical systems [6–8].

As the 3rd generation light sources boosted the first big step in X-ray optics, the Free Electron Laser (FEL) and upcoming Diffraction Limited Storage Rings (DLSR) is unleashing a new one. With coherent sources, the need to preserve the wavefront and, produce diffraction-limited focused spots, seeded the realization of new polishing techniques for optics [9].

The improvements in optical manufacturing have been possible thanks to the simultaneous improvements in optical metrology. Both in- and ex-situ metrology have been receiving more significant investments in recent years than in the previous ones. Ex-situ metrology is still evolving toward sub-nm and nrad precision on assembled mirrors. In-situ metrology is becoming more and more popular, pushing the potential of the new beamlines to their limits.

Moreover, thanks to the improvements in mirror polishing and metrology (dedicated to assembled mirror), it has been possible to produce for the first time an almost perfect out of focus wavefront in an X-ray facility. At LCLS, the development of a stress-free mirror holder coupled with the use of ultra-polished mirror has lead to a remarkable improvement of the quality of the beam, in and out of focus (see Fig. 1), in agreement with the expected performances [10].

Along with hardware developments, software used to model and simulate beamline performance has seen significant growth. The first Ray Tracing Program widely used by the X-ray community was developed by Franco Cerrina and his team at Madison in the Eighties [11]. It has subsequently been adopted worldwide and adapted to different platforms and equipped with user interface. Very recently, advanced programs handling coherent sources and representing a major upgrade to ray tracing, have been realized thanks to collaborative work from different laboratories. Programs like WISE [12,13], Hybrid Shadow [14] and Synchrotron Radiation Workshop (SRW) [15], are friendly, permitting the design of advanced beamlines and the possibility to test novel optical schemes and giving a deeper understanding of their performance.

Hybrid Shadow is an evolution of the well-known Shadow, described earlier. It is based on a "hybrid method" calculating the diffraction effects from an optical element by means of wavefront propagation, and combining the results with ray tracing. In this way, diffraction effects due to clipping or apertures as well as shape errors are taken into account, and can be handled in far and near field. SRW computes the synchrotron radiation from relativistic electrons in the near and far field range. X-ray (as well as longer wavelengths) 2D propagation is implemented by using Fourier Optics and can handle both, partial, and fully coherent radiation.

WISE is a physical optics simulation package used to compute the complex electromagnetic field downstream of one or more optical elements. Originally developed for simulating astronomical telescopes, as many other programs, it has been recently included in the OrAnge SYnchrotron Suite (OASYS) [16], a new graphical environment gathering most of the simulation tools that have been developed and used within the synchrotron and free electron laser community. WISE is designed for use in the operating range from extreme ultraviolet to hard X-rays, at grazing angles of incidence, using spatial and temporal fully coherent sources. At grazing incidence, where the reflection in the XUV range is higher, diffraction is more effective in the incidence plane than in the transverse direction, usually by a factor of 100–1000. This allows the user to neglect the mirror's sagittal error and to consider only the longitudinal profile. The computation of the intensity distribution in the focal plane, or Point Spread Function (PSF), is performed using Kirchhoff's scalar diffraction formula over a 1D domain:

$$PSF(x) = \frac{\Delta R}{E_0^2 \lambda f L^2} \left| \int_{f-L}^{f} E\left(r_h, 0, z_h\right) e^{-i\frac{2\pi}{\lambda}\sqrt{\left\{(x-r_h)^2+z_h^2\right\}}}, dz_h \right|^2$$

where f is the nominal focal distance, $L \ll f$ is the mirror length, ΔR is the maximum–minimum radius, λ is the wavelength of the focused beam and E is the diffracted field on the second mirror at the x–z plane. It is possible to include mirror defects in terms of figure error (measured or calculated) and micro-roughness (though there is no physical distinction between the two, a practical one may exist). Except where explicitly stated, all the simulation shown in this paper has been performed using WISE.

In the following sections, this article will focus on the development in X-ray optics fields that have seen major investments in recent years. Ex- and in-situ metrology and adaptive optics will be discussed including the current achievements and ongoing projects. This is not intended to be an exhaustive lists but an overview biased by the authors involvement and knowledge of how the particular needs have been addressed and solved.

1. Optical metrology

During the past decades, optical metrology has played a major role on the development of synchrotron optics. X-ray mirrors quality has evolved rapidly, accelerated by the development of extremely brilliant 3rd/4th generation synchrotron and Free Electrons Laser (FEL) radiation sources. These X-ray mirrors, planes or off-axis ellipses with lengths of up to 1 m, must preserve the incoming wavefront so they are mainly characterized by residual slope errors in the range of 50 nrad rms or sub nm rms height errors, and 0.3 nm rms or less for micro-roughness [17].

In-situ, at wavelength, metrology became essential for assessing the beamline performances and ex-situ metrology plays the role of achieving the ultimate performance. In the next two sections, these two complementary aspects of mirror and beamline performance characterization will be described.

1.1. Ex-situ metrology

In the field of optical metrology, there are many possible metrology technology solutions with different benefits and shortcomings. Interferometers typically have sub wavelength accuracy but require dedicated designed null optics when the surface under test is not spherical. For measuring grazing incidence optics, those typically used in SR and FEL facilities, the Long Trace Profiler (LTP) is the most commonly used instrument, also the one that started the modern optical metrology technology boom. This is a direct slope measurement device, able to detect slope variations of the order of 0.1 μrad. The Long Trace Profiler (LTP) is based on the principle of the pencil-beam interferometer developed by Von Bieren [18]. The concept of the LTP, very similar to an autocollimator, is simple. A narrow collimated laser beam is sent to the Surface Under Test (SUT) and the variation of the SUT-reflected beam angle is measured by means of a high quality long focal lens and a CCD detector. In this way, by moving the laser beam on the mirror surface, one can reconstruct its slope. In some cases mirrors are specified using height error also, it can be useful for the mirror manufacturer to know the height error when making corrections. This information can be derived from the slope data simply by integration. The first generation surface profiler (or profilometer), referred to above as the LTP, [19–21] was originally developed at Brookhaven National Laboratory (USA) in 1989 to test large plane, spherical and aspherical mirrors. Since its conception the LTP has been adopted by many laboratories around the world and several custom modifications have been implemented. By construction, the system does not need a reference surface, provided the direction of the probe beam is perfectly preserved during the scan. The best translation stages (air-bearing, for example) can have parasitic motion below 10 μrad for a 1 m long translation. This is not sufficient compared to the desired slope resolution. To tackle this problem, the first improvement was made by tracking the optical head tilt with an extra reference beam path. Currently most instruments stabilize their probe beam by scanning only a pentaprism as was first proposed by Qian [22]. The pentaprism maintains a constant angle between the incoming beam, parallel to the translation and the reflected beam directed to the SUT even if the penta-prism is tilted. With the scanning

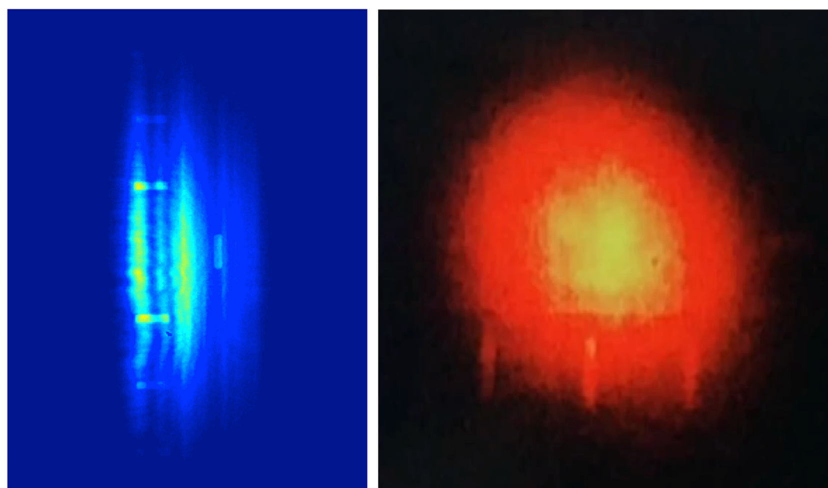

Fig. 1. Measured profile of the LCLS beam before (left) and after (right) the upgrade of the mirrors. The old mirrors, installed in 2009 had shape errors of less than 2 nm rms and were 450 mm long. The new mirrors (installed in 2017) have 0.5 nm rms shape errors and are 1 m long, collecting the entire LCLS HXR beam.

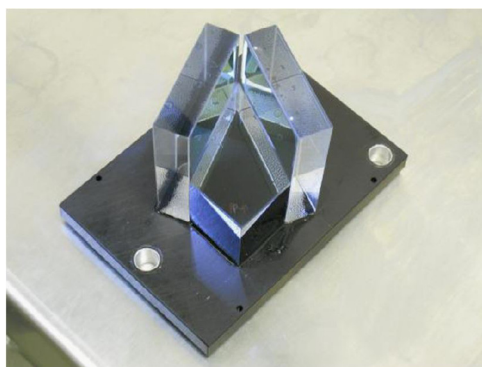

Fig. 2. Hollow Penta Mirrors used in conjunction with a bulk pentaprism to provide the quality of the mirrors and the perfect angle of a pentaprism.
Source: (Courtesy of Shinan Qian BNL/NSLSII).

Fig. 3. NSP and NOM systems at the NSLS II metrology laboratory.

pentaprism (or more recently a penta-mirror or hollow pentaprism, see Fig. 2 [23], the slide pitch error will not influence the output beam direction. Different orientations of the pentaprism combined with a few additional mirrors provide the option to measure the SUT face up, face down or on its side. This can be critical as it allows the mirror to be measured in the same orientation that it will be in when installed in the beamline. This allows optimization of the mechanical mounting (gravity compensator, mirror clamping or cooling for example).

The second generation surface profiler, the Nanometer Optical Measurement machine (NOM) [24–26], developed at BESSY-II (Germany) in 2002, can achieve an accuracy of 50 nrad rms or better for plane or large radius of curvature surfaces. The angle measurements are performed by a commercially available autocollimator, developed for metrology. The spot size of the autocollimator (AC) then determines the lateral resolution. The smallest spot size, which can be achieved with the standard commercially available autocollimator, is about 2–3 mm. The NOM scheme uses a fixed optical head (the ELCOMAT 3000/8 with a 2.5 mm aperture) coupled to a scanning pentaprism. Since the commissioning of the first NOM in Berlin, several systems have been implemented at different laboratories around the world and have reported measurement accuracies below 50 nrad for moderate curvatures (in the km range) and ~200 nrad rms for strongly curved surfaces, down to ~10 m and below [27–32]. Another high accuracy metrology instrument, also based on electronic autocollimators, was developed at the PTB (Germany): the ESAD (Extended Shear Angle Difference) profiler [33].

All of these instruments require precise calibration of the autocollimator for their specific application [34–37]. Most of the ELCOMAT 3000/8 used in slope measuring instruments are calibrated by the PTB with their primary angle-reference standard, a Heidenhain WMT220 angle comparator with a 5 nrad [0.001 arcsec] uncertainty. In the NOM scheme, the distance between the SUT and lens objective varies continuously during the pentaprism scan; also the autocollimator suffer from systematic errors difficult to totally eliminate. One solution to tackle these difficulties was proposed by S. Qian and led to the development of the NanoSurface Profiler (NSP) [38] shown in Fig. 3.

In this case it is possible to use the exact PTB calibration data since the measurement occurs at a same fixed distance. By proper inclusion of the calibration data in the data acquisition, it is possible to achieve sub 50 nrad rms measurement accuracy, even on curved surfaces where the return beam traverses the full 10-mrad acceptance of the NSP.

Recently, a 2D Slope measuring System based on a Stitching Shack Hartmann Optical Head (SSH-OH) aiming to perform 2D high accuracy optical metrology for X-ray mirrors has been proposed. The first idea to use a Shack–Hartmann Wavefront Sensor to characterize X-ray mirror was proposed by Imagine Optic [39] and SOLEIL synchrotron [40,41]. This system was developed to perform high-accuracy automated metrology for extremely high quality optical components needed for SR or

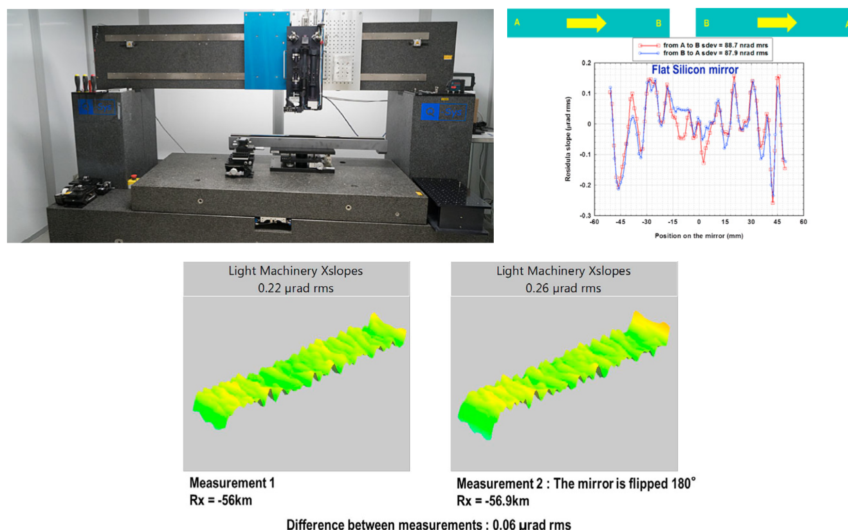

Fig. 4. Top Left: The NSLS II metrology Shack–Hartmann based 2D profilometer. Top Right: An example of high accurate topographic measurement of a mirror by using the Shack–Hartmann system. Bottom: two 2D topographic mirror maps (flipped by 180°) of a flat mirror from the Shack–Hartmann system.

FEL facilities, EUV lithography and X-ray astronomy with slope error accuracy better than 50 nrad rms.

Hartmann methods will be described in the next session, being one of the most accurate methods for at wavelength metrology. We briefly mention here that it measures wavefronts by using an array of sub-apertures. Each sub-aperture defines a pencil of light whose mean direction is the average normal to the wavefront on the sub aperture. Detection of the center of each pencil on an area detector downstream the aperture array allows the reconstruction of the wavefront from its gradient (local slopes). A Shack–Hartmann (SH) sensor is an improved implementation of the method in which the sub aperture array is replaced by an array of micro lenses for better sensitivity [42–44].

The use of a Shack–Hartmann Sensor for mirror metrology provides a measurement of the slope profile of the surface under test by scanning the high accuracy Shack–Hartmann wavefront sensor along the mirror surface. The sensor developed at Imagine Optic uses an 11×15 micro-lens array with 1.2 mm pitch, in a patented rotated square geometry, which eliminates interferences with high order light diffracted by the sub apertures. The sensor light source is a single mode fiber laser diode emitting at 405 nm. The light is collimated by the doublet lens and sent to the SUT by reflection on a beam-splitter. After reflection on the SUT it is analyzed by dedicated ultra high accuracy Shack Hartmann (SH) sensor. The SH sensor mounted on a precise translation stage and an example of 2D topographic map of a mirror are shown in Fig. 4.

The SH head is mounted on a stage and scanned step by step over the SUT, allowing to measure a 13 mm-wide strip area over the length of the mirror and providing a 2D slope map. For the characterization of long mirrors a stitching process has to be applied. The stitching method is based on the well-known concept developed for interferometry [45,46]. It consists of the overlapping of adjacent surface measurements by translation of the optical head or of the SUT. Redundancy of the information is used to subtract most of the systematic errors including measurement errors induced by the imperfections of the translation stage. To optimize the process, the slope measurements in the overlap regions are used in a linear squares fitting routine to determine the relative tilts between frames of data. These relative tilts are then used to correct the data and to construct a stitched 2D gradient map for the SUT. Once the map of the surface gradient is reconstructed, the surface itself is reconstructed using a wavefront reconstruction algorithm such as the one described by Southwell [47–49].

An alternative way of measuring 2D optical surfaces with high accuracy, still under investigation, is by using deflectometric methods. They are capable of providing full-field topography data for specular freeform surfaces and have been developed in the last decade. They have been proven to be successful in various fields of application, such as the measurement of progressive power eyeglasses, painted car body panels, or windshields. This metrology method uses sinusoidal modulations on a digital display (such as an LCD monitor) as a source. Surface measurements are made by imaging the reflection of the display by the surface under test. The source modulation, combined with powerful software, allows an accurate determination of ray trajectories from a particular location on the screen to a point on the SUT, then into the camera aperture. The performance of the phase measuring deflectometry technique implemented originally at the University of Arizona has been impressive. A wide variety of optical surfaces have been measured, from small spheres to an 8-m off axis mirrors. As an example of the test accuracy, measurements from a mirror used for an X-ray synchrotron are shown. In this first attempt at measuring X-ray mirrors, accuracy approaching 1 nm rms was achieved using a computer monitor as the source and a commercial CCD camera as the imager. Subsequent results have shown higher performance (see Fig. 5).

1.2. *In-situ, at wavelength metrology; Wavefront sensing*

In-situ, at-wavelength X-ray wavefront metrology traces its roots to the pioneering work of Linnik [51], and later Speer [52] and Mrowka [53], who demonstrated a common-path *point-diffraction interferometer* for X-ray optics testing. The principle was also demonstrated by Goldberg [54] for EUV wavelengths. X-ray in-situ metrology allows test of complex optical systems in real conditions and the optimization of beamlines with the X-ray beam. Measuring the effect of the optics on the beam at the operative wavelength, gives the information that is really needed to understand the performance of a particular optical system. For this purpose, several diagnostics have been developed, capable of providing different information about multiple characteristics. In particular, it is possible to determine the beam transverse profile, the intensity, the trajectory, the spectral content, and so on. These diagnostics provide all of the information needed to operate a non-diffraction limited beamline. For FEL or DLSR, it becomes essential to use in-line (semi-non-invasive) and possibly shot-by-shot diagnostics, able to measure parameters never considered before. Beamlines designed for advanced experiments are becoming increasingly sophisticated, and aim to probe the smallest scales, both spatial and temporal, of interesting and promising new materials. Consequently, the requirements on the performance of X-ray optics are progressively becoming more stringent, especially with respect to the mirrors focusing the light onto the sample.

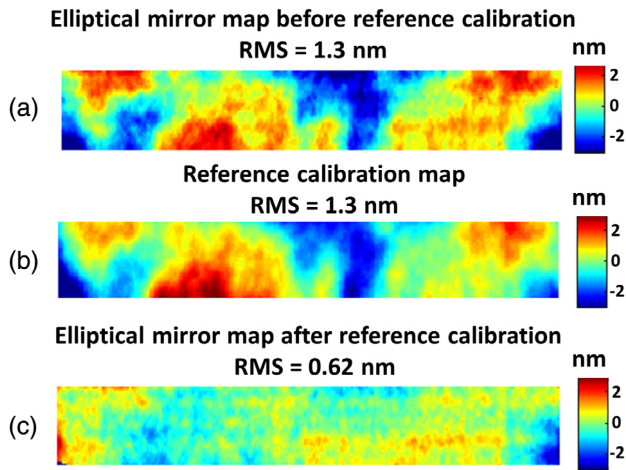

Fig. 5. Example of measurements of a mirror used for an X-ray synchrotron using deflectometry. (a) Measured surface irregularity of the elliptical mirror before reference calibration applied, rms = 1.3 nm; (b) averaged calibration map with translation of reference flat, rms = 1.3 nm; and (c) surface map of elliptical mirror with calibration of reference applied, rms = 0.62 nm [50].

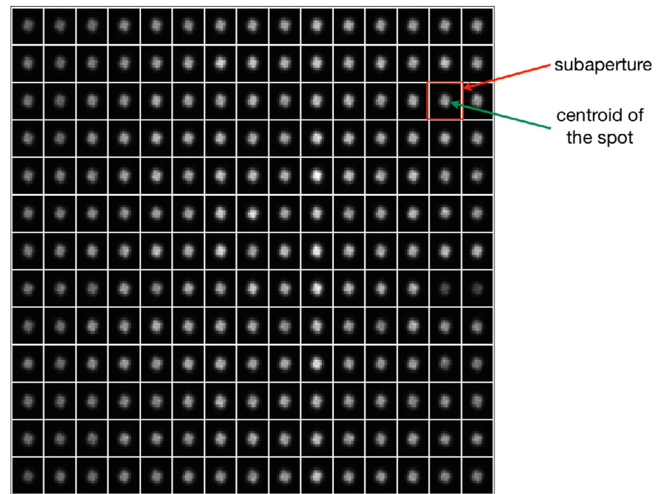

Fig. 7. The individual point spread functions of the quadratic sub apertures extend to the boundaries of the subapertures in the horizontal and vertical directions, respectively.

Although the fabrication and the optical metrological characterization methods have progressed significantly in recent years, the degradation of the performance of these optics, due to aging, contamination, drift and mechanical instability, remains an open issue. For this reason scientists are developing comprehensive methodologies for in-situ alignment and tuning of focusing mirrors. This is especially true for optical systems intended to shape the beam, not just focus it.

Several methods for tuning (i.e., aligning and obtaining the best focus) active optics systems by reducing the wavefront aberrations have been developed in both the hard and soft X-ray regimes [55–57]. These methods have been assisted by rigorous computational modeling of the optical systems [58–60].

Wavefront sensing is the technique that has seen the largest development in recent years. This technique can actually be applied to both "standard" and active optics systems. In the former case the achievable goal is the full exploitation of the optical characteristics of the (focusing) mirrors by minimizing all the possible source of aberrations coming from non-perfect alignment. In the latter case, the possibility of actively modifying the mirror shape lets the user perform a detailed and thorough optimization of all mirror parameters, from alignment (position, angles, etc.) to shape (curvature). This is especially important when focusing configurations different from the nominal are used (e.g., request of variable spot size, focusing on different endstation positioned sequentially, and so on…). The most commonly used techniques are Talbot and Shearing interferometry and Hartmann-based wavefront sensing.

Grating shearing interferometers offer some advantages for short-wavelength applications. They use a 1D or 2D grating placed in a converging or diverging beam path. The Talbot condition guarantees that certain longitudinal planes will produce high contrast fringes on a downstream detector. Shearing offers simple alignment, high efficiency, and easy data analysis.

Talbot interferometers [61,62] consist of two gratings in sequence, where the downstream grating is placed in a Talbot, self-focusing plane of the upstream grating, and creates a high-contrast Moiré with a significantly lower spatial frequency than the grating pitch. To improve the sensitivity, the second grating is slightly rotated [63]. A single-shot, 2D, single-grating interferometer (similar to grating shearing) has been used as feedback for an adaptive HXR mirror system [64].

The Hartmann Wavefront Sensors has been explored by a number of laboratories [55,65,66] and, at least, one commercial vendor (Imagine Optic). It measures wavefront slopes non-interferometrically using a hole-grid placed in the beam path, by employing a principle attributed to Hartmann [ca. 1902].

The gradient of the local wavefront impinging on the holes determines the propagation angle of each beamlet onto a downstream detector, where they are measured individually. The classical Hartmann setup is described comprehensively in Fig. 6. If the measurement is performed very carefully, the accuracy of the method is quite high and comparable to interferometry.

The Hartmann sensor has some special properties: the measurement is almost independent of the degree of coherence, partially coherent

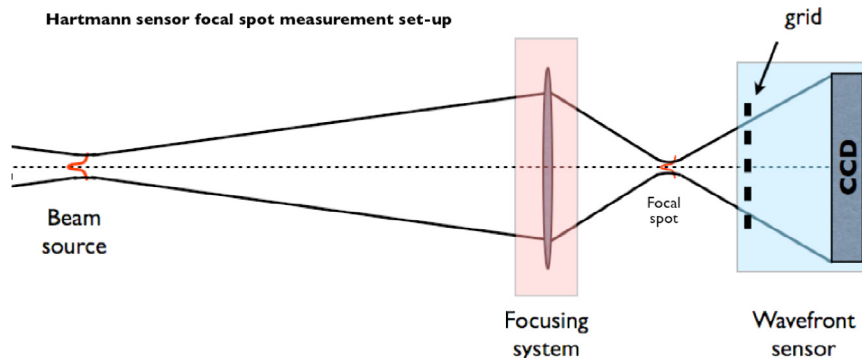

Fig. 6. Hartmann sensor measurement set-up for a focusing system. The Sensor is located after the focal plane.

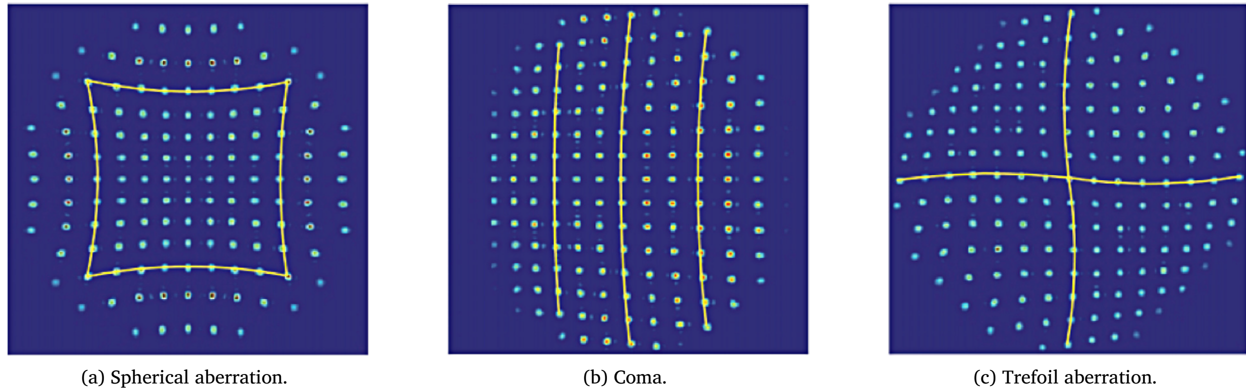

Fig. 8. Three particular cases of wave aberrations as measured by a wavefront sensor.

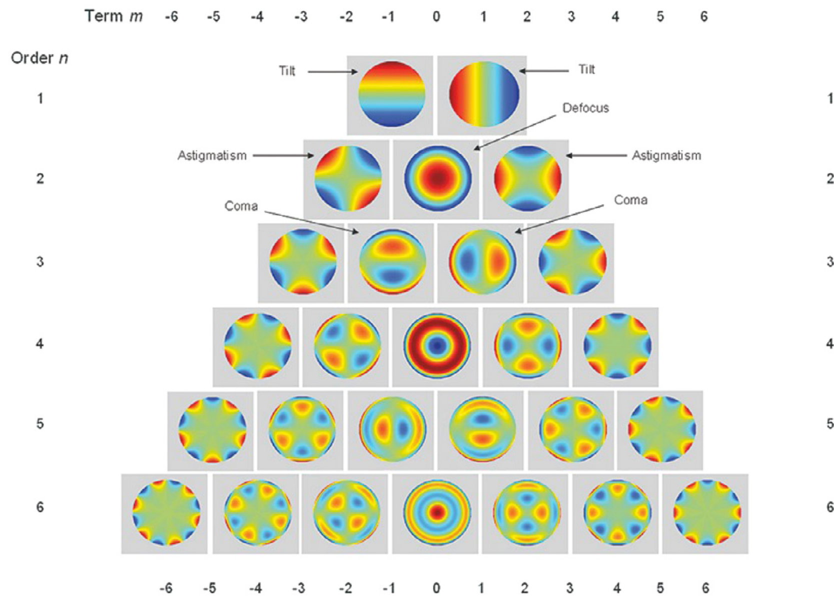

Fig. 9. The measured wavefront can be decomposed into a linear combination of Zernike polynomials that describe typical optical properties and errors of the optical system. The polynomial decomposition gives a numerical representation of any kind of aberration of the sample. The Zernike polynomials are a set of orthogonal polynomials on a unit circle that work very well to describe a surface, representing the constant phase surface of an optical wavefront. The picture shows the first 27 Zernike polynomial terms.

beams can be analyzed as well as coherent beams, the spectral sensitivity is primarily dependent on the properties of the CCD sensor, and there is no dependence on the polarization properties of the incoming light.

Since the pinholes constituting the Hartmann mask have a finite size, this leads to macroscopic spots of light in the measuring planes. These spots are photometrically evaluated in order to determine their centroids, and the deviation of a centroid from its ideal nominal position gives the lateral deviation, which is assigned to the central ray within the corresponding pinhole. This means that the aberration is averaged across the single pinhole area and the error contribution of each finite-sized hole depends on its relative size and the gradients of the wave to be measured.

The main parameters of the Hartmann system are: (1) number of pinholes, (2) geometry of pinhole grid, (3) diameter of pinholes, and 4) locations of measuring planes.

If the pinholes are chosen to be very small, one has the advantage of a very accurate local definition of the wavefront derivative in the center point of the subaperture. But, if the holes are too small there is a diffraction effect, which causes a large spreading of the projected beam on the detector plane. If the individual pinhole beams are no longer separated in the back measuring plane, the calculation of the centroid is impossible or at least becomes erroneous due to a crossover of energy between the channels. If the pinholes are quite large in diameter, the wavefront aberrations across this finite size cause an additional broadening.

The centroid position of each spot is proportional to the inclination of the average wavefront in the corresponding subaperture and can be evaluated accordingly. The spots are detected by a two-dimensional sensor, which determines the centroid position in both vertical and horizontal coordinates, and these positions are then analyzed. Fig. 7 shows a typical spot pattern of a sensor. The diameter of the beam is adapted to the size of the sensor; typically a fill factor of 70%–90% is desired. The shape of the sub-apertures is square. Circular apertures and hexagonal grid geometries are also possible, but the simplest arrangement is Cartesian.

If the incoming beam suffers from wave front aberrations, there will be a deformation in the grid of the spots in the image plane. In particular, for some simple aberration types, one observes characteristic patterns such as those shown in Fig. 8. The yellow lines help to identify the deformation of the grid lines in the spot pattern. The deviations from a rigid Cartesian shape describe the centroid offsets due to the aberrations.

The evaluation of the Hartmann test uses the relationship between the wave aberration W and the transverse aberrations $\Delta x'$, $\Delta y'$. Where

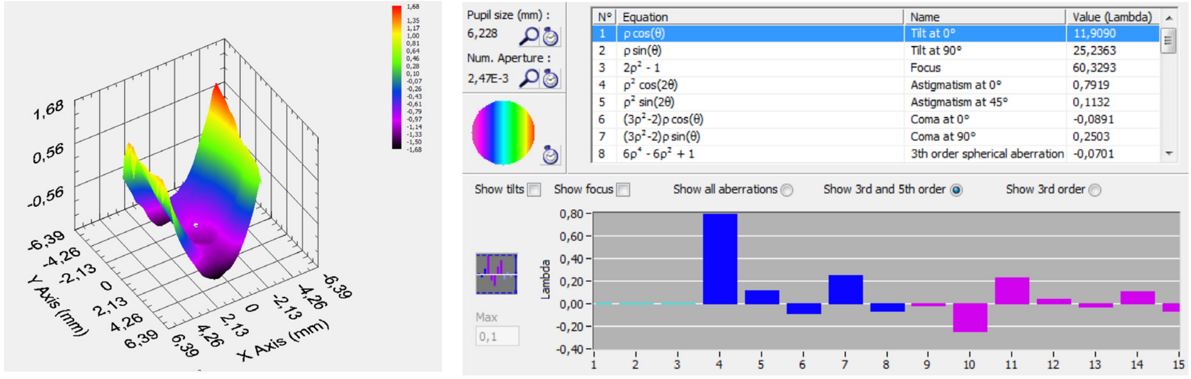

Fig. 10. Left panel, the picture shows the residual wavefront measured by the Hartmann sensor of a K–B active optics system at 20 nm wavelength, which is the difference between the actual wavefront (tilt corrected) and the ideal wavefront (a spherical wave). Z-axis is in unit of lambda. Right panel, the picture shows the Zernike parameters related to the wavefront measured.

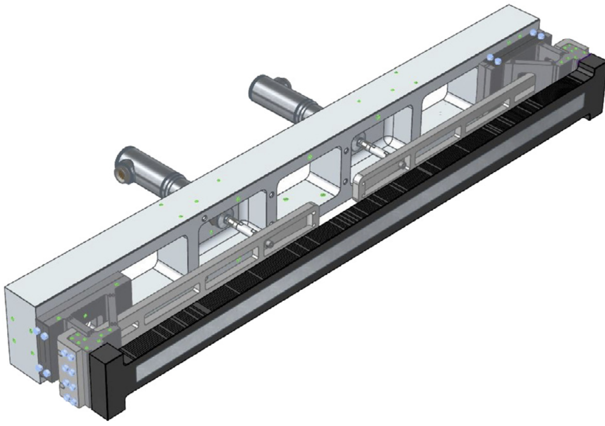

Fig. 11. Mirror bender without cooling in horizontal deflecting configuration.

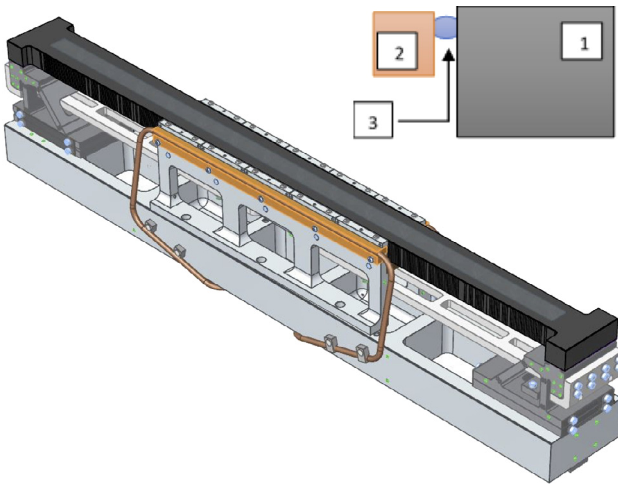

Fig. 12. Top right: Schematic representation of cooling scheme. The mirror (1) thermally coupled to the cooling block (2) with GaIn (3). Center: Mirror bender with cooling in vertical deflecting configuration.

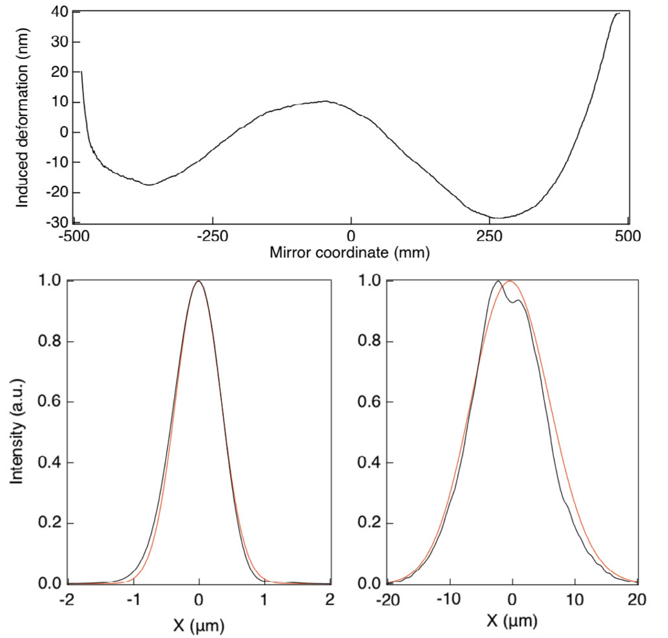

Fig. 13. TOP: measured effect of the GaIn when the mirror is bent to it is extreme position for a 2 m focal distance. BOTTOM: Simulation of the expected performances of a 2 m focal distance mirror at 900 eV with (black) and without (red) the GaIn. The simulations have been performed in focus (left) and 20 mm out of focus (right). (For interpretation of the references to color in this figure legend, the reader is referred to the web version of this article.)

$\Delta x'$ is the horizontal aberration and $\Delta y'$ is the vertical aberration.

$$\Delta x' = -R\frac{\partial W(x,y)}{\partial x}, \quad \Delta y' = -R\frac{\partial W(x,y)}{\partial y}$$

If R is the radius of the reference sphere, the equations connect the measured deviations to the wavefront in air. These two equations are given in matrix form, because the centroid offsets are known from the measurement of every pinhole center coordinate. The integration of these equations can be done locally according to

$$W(x,y) = -\frac{1}{R}\int_0^x \Delta x' dx - \frac{1}{R}\int_0^y \Delta y' dy$$

Another possibility is a polynomial fit of the gradient fields, followed by analytical integration. For example, it is possible to use the Zernike polynomials and to express the coefficients as a weighted sum over all pinhole contributions in the following equation:

$$C_{nm} = \frac{\sin u'}{\lambda}\sum_j g_{nmj}^{(x)}\Delta x'_j + g_{nmj}^{(y)}\Delta y'_j$$

Expressing the wavefront data in the Zernike polynomial form, aids the interpretation of wavefront deformation. The measured wavefront is decomposed into a linear combination of Zernike polynomials, which

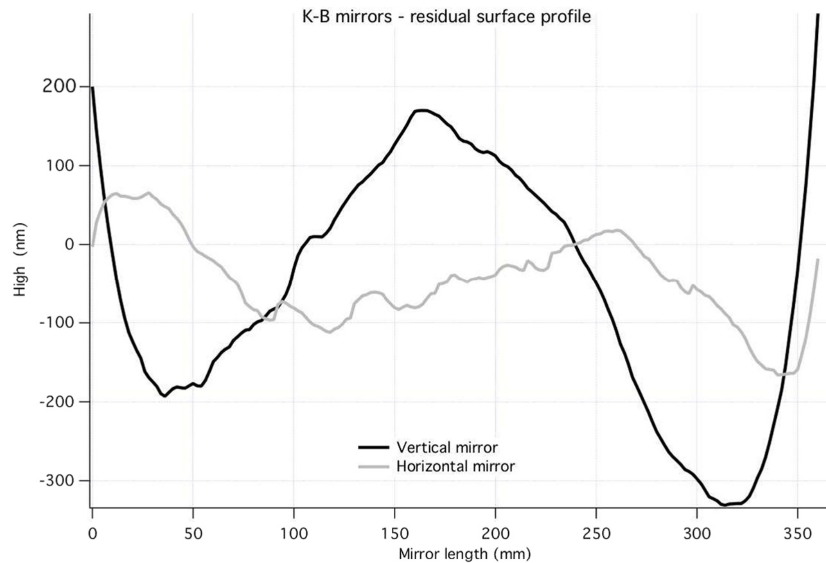

Fig. 14. Residual surface profiles obtained by subtracting the measured and the ideal elliptical profile for the two mirrors forming the FERMI K–B system.

describe typical optical properties, and errors of the optical system. The most common aberration terms are highlighted in Fig. 9. The polynomial decomposition gives a numerical representation of any kind of aberration of the sample.

To discuss a real application, let us consider a recent example of optimization performed at the FERMI FEL in Trieste, Italy. The system to optimize is a Kirkpatrick–Baez active optics system [67–69]. The system will be described in the next section. In order to describe the optimization process, let us consider the first eight Zernike parameters that correspond to eight parameters of the system: pitch, roll, and bender actuation (two) for each of the two mirrors, (a total of eight degree of freedom).

Fig. 10 left, shows the residual wavefront measured by the Hartmann sensor, that is, the difference between the actual wavefront (tilt corrected) and the ideal wavefront (a spherical wave).

The residual wavefront (flat in the ideal case) presents an rms around 0.7 unit of lambda, considerably high value. Fig. 10 right, shows the Zernike parameters related to that wavefront reconstruction. Two Zernike parameters are out of specification: the number 4, corresponding to the astigmatism at 0 degrees, and the number 7, the coma at 90 degrees. Both are visible in the wavefront surface.

From the measurement of the wavefront one can back propagate the electric field and reconstruct the focal spot. In the next section we will show how accurate this method can be in predicting the actual spot profile.

2. Active optics

When active optics reached the Synchrotron Radiation community, it was mainly due to the need to compensate thermal deformations. When the brightness of SR and FEL Light sources increased and the emittance decreased, sub-micron focused beams became feasible. With this new possibility a second generation of active optics was born. These systems, typically consisting of two-actuator benders provided control of higher order aberrations that allowed for a closer approximation of the “perfect” tangential. To achieve the smallest possible focus, the focusing mirrors are usually mounted in the so-called Kirkpatrick–Baez configuration [70]. Two tangential elliptical (or spherical) mirrors, are mounted at 90° with respect to each other, so one mirror focuses horizontally and the other vertically. This configuration gives the flexibility to compensate for any initial astigmatism of the beam and correct for beamline error in the two orthogonal directions. Still, because of the limited polishing precision, it has not been possible to obtain diffraction-limited spot in the Soft X-rays in the past. In the Hard X-ray thanks to the smaller beam divergence and, therefore, shorter mirrors, some outstanding results, mostly at Spring-8, Japan, have been achieved [71–75].

Despite the improvement of both polishing techniques and metrology, a uniform beam out of focus, was almost impossible to realize. One of the very first example of almost perfectly uniform beam, out of focus, in the Hard X-ray, is shown in Fig. 1 of this article, realized at the LCLS FEL light source after the 2017 mirror system upgrade. The challenge in achieving a uniform beam out of focus is due to high frequency polishing errors, which cannot be compensated for with two-actuator benders. To compensate high spatial frequency errors, some multi actuators mirror systems have been developed and, in some cases, successfully implemented on SR beamlines [76,77]. These systems usually work in cases where the beam is monochromatic and/or low power. With the advent of nearly monochromatic light sources (FELs) and high brilliance Synchrotrons this problem must be solved for the case of high heat load optics. The LCLS-II project will add a high repetition rate superconducting accelerator, along with new undulators to the existing LCLS FEL. The soft X-ray (SXR) beam line will operate in the energy range, 280–1300 eV, at up to 1 MHz repetition rate. The Source is almost monochromatic and nearly the full source power will be transported down to the sample. Therefore, the bendable focusing mirror system, operated in a Kirkpatrick–Baez configuration needs to be cooled.

High force in vacuum actuators is used to bend the mirror, shown in Fig. 11. To minimize the force necessary to bend the mirror, long lever arms apply a force to the flexures. The long lever arms are designed to be compliant which increases the resolution of the bender and minimizes the effects of thermal expansion. Flexure based four-bar linkages allow the actuator forces to be converted almost entirely into bending moments at the neutral bending axis of the mirror. This limits the amount of tensile force loading that the mirror experiences. To maximize the useful region of the mirror, the ends are epoxy bonded. The epoxy joint design minimizes tensile loading in the epoxy and therefor maximizes its performance. A flexure based twist correction mechanism removes twist induced during assembly.

The use of a Gallium Indium (GaIn) liquid metal thermal interface, as shown in Fig. 12, mechanically decouples the cooling system from the mirror. Although this method has been widely used in the synchrotron community, little is known about the mechanical properties of the eutectic or how a system should be designed for optimum mechanical

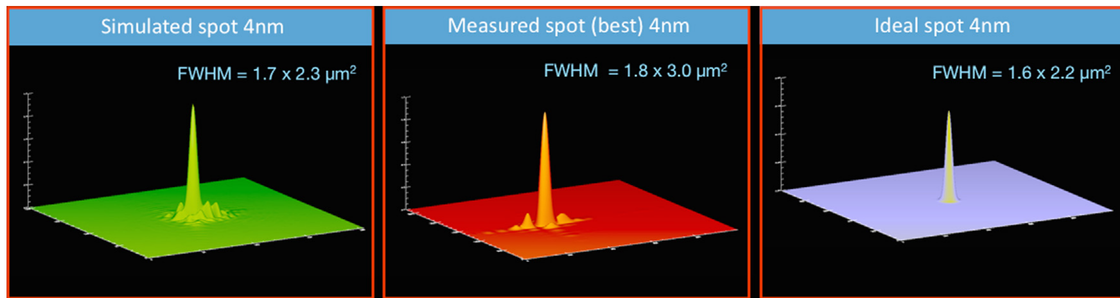

Fig. 15. Simulation and reconstruction of the spot profile in the DiProi experimental chamber. Left: Simulation (using WISE) of the spot profile including the measured shape errors; CENTER: Spot profile reconstructed after the wavefront sensor measurements; RIGHT: simulation of the spot in the case of perfect mirrors.

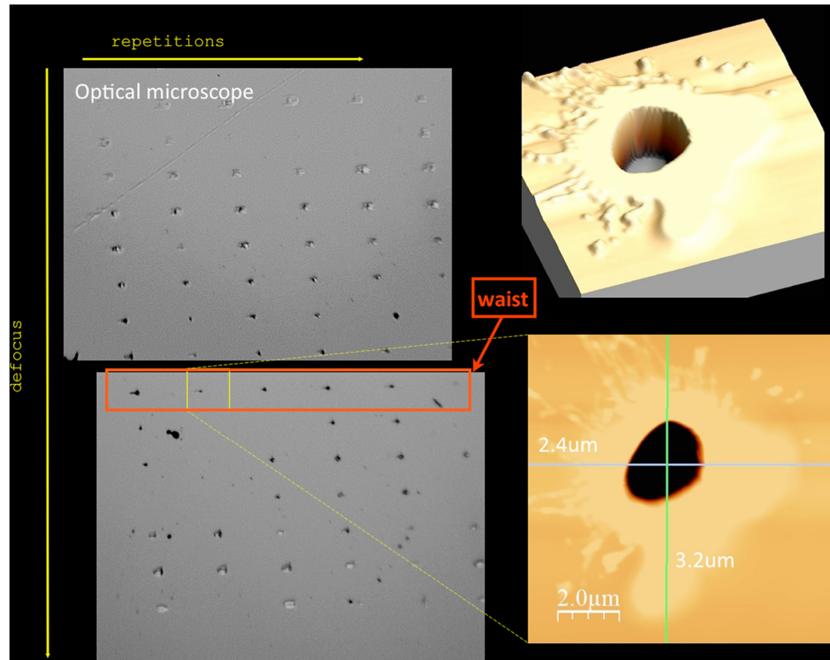

Fig. 16. The two gray plots on the left show the imprint of the focal spot at 4.1 nm wavelength seen by an optical microscope. The horizontal direction represents the repetitions, shot by shot, and the vertical direction represents defocus. The position highlighted with the red square represents the waist. We analyzed one of these shots with an AFM (right hand plots) and we obtained a spot size estimation of $2.4 \times 2.5\ \mu m^2$. In this kind of measurements it is very important to carefully tune the intensity of the beam, high enough to ablate, low enough not to melt. Since in this case some melting effect is present, we have to consider this result as an upper limit.

decoupling. A series of tests performed at the SLAC National Accelerator Laboratory begin to shed some light on this.

As one might expect, force coupling of the GaIn is directly related to the interface thickness, the gap between the cooling and the mirror. With a thick enough gap, mechanical coupling approaches negligible, but the stability of the GaIn becomes problematic. Since the GaIn is only held in place by surface tension, stability is very important. A number of potential interfaces thicknesses have been chosen for further study and optimization. Early prototype testing results are very promising as they show negligible effects from the GaIn if the gap is maintained above 100 μm. The measured induced deformation, for a 1 m long mirror and 100-μm gap, as well as the expected performance, in and out of focus, is shown in Fig. 13.

Another example of a mirror bender is the Kirkpatrick–Baez Active Optics System developed for the FERMI FEL facility. It is an example of an "evolving design" that has been tested and developed continuously between 2012 and 2014 using FEL radiation. After several experimental shifts dedicated to the characterization of such systems, the performance in terms of spot sizes and shapes has almost reached their nominal opto-mechanical limits. Spots as small as $1.8 \times 3.1\ \mu m^2$ have been obtained by taking advantage of several diagnostics such as wavefront sensors, YAG and phosphor screens and damage on PMMA and silicon substrates.

The two mirrors, forming the K–B system, have been characterized by using a Long Trace Profiler (LTP) at the Optical Metrology Laboratory of Elettra-Sincrotrone Trieste. Applying the Adaptive Correction Tool software (ACT) [78], the mirrors have reached the best profiles that this mechanical system can provide. This is close to the nominal ellipsis, the horizontal mirror having a central sagitta of about 360 μm, and the vertical mirror having a central sagitta of about 230 μm. A description of the mechanical system can be found in literature [79,80].

The ACT software calculates the interaction matrix of the mirror bending using the least squares approach. The interaction matrix is then used to calculate the steps to be given at each motor to shape the mirror as close as possible to a desired profile.

This iterative procedure converges very quickly to reach the needed quasi-elliptical mirror profile or another desired shape. The difference between the ideal target shape of each mirror and the actual measured shape is shown in Fig. 14.

These mirrors have been installed and tested at the DiProi beamline of FERMI. The optimization of the mirrors has been performed by measuring the wavefront with a Hartmann sensor similarly to what

described in the previous Section 1.2. As described earlier, the wavefront sensor software provides the intensity distribution of the beam. This is a combination of the several modes resulting in a "noisy hyper-Gaussian" intensity profile, and the wavefront residuals from ideal propagation from the tilted pinholes of the array plate. Combining these two measurements it is possible to obtain the electric field (sampled with a number of points equal to the number of pinholes in the 15 mm-array plate). This permits reconstruction of the focal spot and, therefore, optimization of the mirrors, by back-propagating the electric field from the Hartmann grid to the focal position.

To optimize the curvature of the mirrors, the Zernike coefficients associated to the aberrations correctable by the mirror mechanics, have to be minimized. Fig. 15 shows the best focal spot achieved at 4 nm photon wavelength ($FWHM = 1.8 \times 3.0$ μm^2) calculated by reconstruction from Wavefront sensor measurements. It is compared with the simulations (using the previously described WISE program) for ideal mirrors (no shape errors) and including the actual measured profile as shown in Fig. 14.

To cross check the results obtained with the wavefront sensor, a series of measurements of ablation imprints on a 500 nm PMMA sample at several fluences, have been conducted. The best shot in the line of the waist (see Fig. 16), measured by an Atomic Force Microscope, gives a spot estimation of about 2.4×3.2 μm^2. In this kind of measurements it is very important to carefully tune the intensity of the beam; it must be high enough to ablate the PMMA, but low enough that it does not melt the sample. In this case some melting effect are present (as clearly seen in Fig. 16). This introduces uncertainty in the spot measurements and an overestimation of the beam dimensions. Nonetheless, is the ablation measurements are in very good agreement with the spot reconstructed by using the Hartmann Sensor.

Acknowledgments

L.R. and M.Z. acknowledge the support and help from the entire FERMI team, and in particular from the staff of the FERMI experimental endstations.

This work is partially performed under the auspices of the U.S. Department of Energy by BNL under Contract No. DE-SC0012704, and SLAC under Contract No. DE-AC02-76SF00515. The FERMI project at Elettra—Sincrotrone Trieste is supported by MIUR under grants FIRB-RBAP045JF2 and FIRB-RBAP06AWK3.

References

[1] W. Chao, J. Kim, S. Rekawa, P. Fischer, E.H. Anderson, Demonstration of 12 nm resolution Fresnel zone plate lens based Soft X-ray microscopy, Opt. Express 17 (2009) 17669–17677.
[2] I. Mohacsi, et al., Interlaced zone plate optics for hard X-ray imaging in the 10 nm range, Sci. Rep. 7 (2017) 43624.
[3] C. Chang, A. Sakdinawat, Ultra-high aspect ratio high-resolution nanofabrication for hard X-ray diffractive optics, Nature Commun. 5 (2014) 4243.
[4] P.Z. Takacs, S.N. Qian, Design of a long trace surface profiler, Proc. SPIE 749 (1987) 59–64.
[5] H. Yan, R. Conley, N. Bouet, Y.S. Chu, Hard x-ray nanofocusing by multilayer Laue lenses, J. Phys. D: Appl. Phys. 47 (2014) 263001.
[6] D. Cocco, M. Marsi, M. Kiskinova, K.C. Prince, T. Schmidt, S. Heun, E. Bauer, Microfocusing VLS grating-based beamline for advanced microscopy, Proc. SPIE 3767 (1999) 271–279.
[7] R. Reininger, A.R.B. de Castro, High resolution, large spectral range, in variable-included-angle soft X-ray monochromators using a plane VLS grating, Nucl. Instrum. Methods Phys. Res. A 538 (2005) 760–770.
[8] D. Cocco, R. Abela, J.W. Amann, K.P. Chow, P.J. Emma, Y. Feng, G.L. Gassner, J.B. Hastings, P.A. Heimann, Z. Huang, N.M. Kelez, H. Loos, P.A. Montanez, D.S. Morton, H.D. Nuhn, D.F. Ratner, L.N. Rodes, U. Flechsig, J.J. Welch, J. Wu, The optical design of the soft x-ray self seeding at LCLS, Proc. SPIE 8849 (2013) 88490A.
[9] M. Kanaoka, C. Liu, K. Nomura, M. Ando, H. Takino, Y. Fukuda, Y. Mori, H. Mimura, K. Yamauchi, Processing efficiency of elastic emission machining for low-thermal-expansion material, Surf. Interface Anal. 40 (2008) 1002–1006.
[10] T. Pardini, A. Aquila, S. Boutet, D. Cocco, S.P. Hau-Riege, Numerical simulation of the hard X-ray pulse intensity distribution at the Linac Coherent Light Source, J. Synchrotron. Rad. 24 (2017) 738–743.
[11] B. Lai, F. Cerrina, SHADOW: A synchrotron radiation ray tracing program, Nucl. Instrum. Methods Phys. Res. A 246 (1986) 337–341.
[12] L. Raimondi, D. Spiga, Mirrors for X-ray telescopes: Fresnel diffraction-based computation of point spread functions from metrology, Astron. Astrophys. 573 (2015) A22.
[13] L. Raimondi, C. Svetina, N. Mahne, D. Cocco, A. Abrami, M. De Marco, C. Fava, S. Gerusina, R. Gobessi, F. Capotondi, E. Pedersoli, M. Kiskinova, G. De Ninno, P. Zeitoun, G. Dovillaire, G. Lambert, W. Boutu, H. Merdji, A.I. Gonzalez, B. Mahieu, D. Gauthier, M. Zangrando, Microfocusing of the FERMI@Elettra FEL beam with a K-B active optics system: spot size predictions by application of the WISE code, Nucl. Instrum. Methods Phys. Res. A 710 (2013) 131–138.
[14] X. Shi, R. Reininger, M. Sanchez del Rio, L. Assoufid, A hybrid method for X-ray optics simulation: combining geometric ray-tracing and wavefront propagation, J. Synchrotron. Rad. 21 (2014) 669–678.
[15] O. Chubar, P. Elleaume, Accurate and efficient computation of Synchrotron Radiation in the near field region, in: Proc. of the EPAC98 Conference, 1998, pp. 1177–1179.
[16] M. Sanchez del Rio, L. Rebuffi, J. Demšar, N. Canestrari, O. Chubar, A proposal for an open source graphical environment for simulating X-ray optics, Proc. SPIE 9209 (2014) 92090X.
[17] H. Mimura, et al., Focusing mirror for x-ray free-electron lasers, Rev. Sci. Instrum. 79 (2008) 083104.
[18] K. Von Bieren, Pencil beam interferometer for aspheric optical surfaces, Proc. SPIE 343 (1982) 101–108.
[19] P.Z. Takacs, S.N. Qian, US patent No.U4884697, 1989.
[20] P.Z. Takacs, K. Furenlid, R. DeBiasse, Surface topography measurements over the 1 meter to 10 micrometer spatial period bandwidth, Proc. SPIE 1164 (1989) 203–211.
[21] P.Z. Takacs, et al., Long trace profile measurements on cylindrical aspheres, Proc. SPIE 966 (1988) 354–364.
[22] S.N. Qian, W. Jark, P.Z. Takacs, Rev. Sci. Instrum. 66 (1995) 2562–2569.
[23] S.N. Qian, L. Wayne, M. Idir, Nano-accuracy measurements and the surface profiler by use of Monolithic Hollow Penta-Prism for precision mirror testing, Nucl. Instrum. Methods A 759 (2014) 36–43.
[24] H. Lammert, T. Noll, T. Schlegel, F. Siewert, T. Zeschke, Patentschrift DE10303659 B4, 2005.
[25] F. Siewert, T. Noll, T. Schlegel, T. Zeschke, H. Lammert, The nanometer optical component measuring machine: a new sub-nm topography measuring device for X-ray optics at BESSY, AIP Conf. Proc. 705 (2004) 847–850.
[26] F. Siewert, H. Lammert, T. Noll, T. Schlegel, T. Zeschke, T. Hänsel, A. Nickel, A. Schindler, B. Grubert, C. Schlewitt, Advanced metrology: an essential support for the surface finishing of high performance x-ray optics, Proc. SPIE 5921 (2005) 592101.
[27] S.G. Alcock, K.J.S. Sawhney, S. Scott, U. Pedersen, R. Walton, F. Siewert, T. Zeschke, T. Noll, H. Lammert, The Diamond-NOM: A non-contact profiler capable of characterizing optical figure error with subnanometre repeatability, Nucl. Instrum. Methods A 616 (2010) 224–228.
[28] S.K. Alcock, K.J.S. Sawhney, S. Scott, The Diamond-NOM: A non-contact profiler capable of characterizing optical figure error with sub-nanometre repeatability, Nucl. Instrum. Methods Phys. Res. A 616 (2010) 224–228.
[29] V.V. Yashchuk, S. Barber, E.E. Domning, J.L. Kirschman, G.Y. Morrison, B.V. Smith, F. Siewert, T. Zeschke, R. Geckler, A. Just, Sub-microradian surface slope metrology with the ALS Developmental Long Trace Profiler, Nucl. Instrum. Methods A 616 (2010) 212–223.
[30] L. Assoufid, N. Brown, D. Crews, J. Sullivan, M. Erdmann, J. Qian, P. Jemian, V.V. Yashchuk, P.Z. Takacs, N.A. Artemiev, D.J. Merthe, W.R. McKinney, F. Siewert, T. Zeschke, Development of a high-performance gantry system for a new generation of optical slope measuring profilers, Nucl. Instrum. Methods A 710 (2013) 31–36.
[31] S.N. Qian, B. Gao, Nano-accuracy measurement technology of optical-surface profiles, Proc. SPIE 9687 (2016) 96870E.
[32] V.V. Yashchuk, et al., Sub-microradian surface slope metrology with the ALS Developmental Long Trace Profiler, Nucl. Instrum. Methods A 616 (2010) 212–223.
[33] R.D. Geckeler, ESAD shearing deflectometry: Potentials for synchrotron beamline metrology, Proc. SPIE 6317 (2006) 63171H/1–12.
[34] R.D. Geckele, I. Weingartner, A. Just, R. Probst, Use and traceable calibration of autocollimators for ultra-precise measurement of slope and topography, Proc. SPIE 4401 (2001) 184–195.
[35] A. Just, M. Krause, R. Probst, R. Wittekopt, Calibration of high-resolution electronic autocollimators against an angle comparator, Metrologia 40 (2003) 288–294.
[36] T. Yandayan, B. Ozgur, N. Karaboce, O. Yaman, High precision small angle generator for realization of si unit of plane angle and calibration of high precision autocollimators, Meas. Sci. Technol. 23 (2012) 094006.
[37] R.D. Geckeler, M. Krause, A. Just, O. Kranz, H. Bosse, New frontiers in angle metrology at the PTB, Measurement 73 (2015) 231–238.
[38] S.N. Qian, M. Idir, Innovative nano-accuracy surface profiler for sub-50 nrad rms mirror test, Proc. SPIE 9687 (2016) 96870D-1-10.
[39] https://www.imagine-optic.com/.
[40] J. Floriot, X. Levecq, S. Bucourt, M. Thomasset, F. Polack, M. Idir, P. Mercère, T. Moreno, S. Brochet, A Shack-Hartmann measuring head for the two-dimensional characterization of X-ray mirrors, J. Synchr. Rad. 15 (2008) 134–139.

[41] J. Floriot, X. Levecq, S. Bucourt, M. Thomasset, F. Polack, M. Idir, P. Mercère, S. Brochet, T. Moreno, Surface metrology with a stitching Shack-Hartmann profilometric head, Proc. SPIE 6616 (2007) 66162A.

[42] R.V. Shack, Production and use of a lenticular hartmann screen, J. Opt. Soc. Amer. 61 (1971) 656–660.

[43] B.C. Platt, R. Shack, History and principles of Shack-Hartmann wavefront sensing, J. Refract. Surg. 17 (2001) S573–S577.

[44] D. Malacara-Doblado, I. Ghozeil, Hartmann, Hartmann-Shack, and other screen tests, in: D. Malacara (Ed.), Optical ShopTesting, Wiley, 2007, pp. 361–397.

[45] J. Fleig, P. Dumas, P.E. Murphy, G.W. Forbes, An automated subaperture stitching interferometer workstation for spherical and aspherical surfaces, Proc. SPIE 5188 (2003) 296–307.

[46] J.H. Burge, C. Zhao, Applications of subaperture stitching interferometry for very large mirrors, Proc. SPIE 8450 (2013) 84500X.

[47] W.H. Southwell, Wave front estimation from wave front slope measurements, J. Opt. Soc. Amer. 70 (1980) 998–1006.

[48] L. Huang, M. Idir, C. Zuo, K. Kaznatcheev, L. Zhou, A. Asundi, Comparison of two-dimensional integration methods for shape reconstruction from gradient data, Opt. Lasers Eng. 64 (2015) 1–11.

[49] S. Ettl, J. Kaminski, M.C. Knauer, G. Häusler, Shape reconstruction from gradient data, Appl. Opt. 47 (2008) 2091–2097.

[50] R.H. Peng Su, J.H. Burge, L. Huang, M. Idir, High-accuracy aspheric x-ray mirror metrology using software configurable optical test system/deflectometry, Opt. Eng. 54 (2015) 084103.

[51] V.P. Linnik, Akad. Nauk. SSSR Dokl. 1 (1933) 18–23.

[52] R.J. Speer, M. Chrisp, D. Turner, S. Mrowka, K. Tregidgo, Grazing incidence interferometry: the use of the linnik interferometer for testing image-forming reflection systems, Appl. Opt. 18 (1979) 2003–2012.

[53] S. Mrowka, W. Harris, R.J. Speer, Short wavelength interferometric testing of x-ray optics, Proc. SPIE 316 (1981) 16–20.

[54] K.A. Goldberg, R. Beguiristain, J. Bokor, H. Medecki, D.T. Attwood, K. Jackson, E. Tejnil, G.E. Sommargren, Progress towards $\lambda/20$ extreme ultraviolet interferometry, J. Vac. Sci. Technol. B 13 (1995) 2923.

[55] P. Mercère, et al., Hartmann wave-front measurement at 134 nm with $\lambda_{EUV}/120$ accuracy, Opt. Lett. 28 (2003) 1534–1536.

[56] P. Mercère, et al., Automatic alignment of a Kirkpatrick-Baez active optic by use of a soft-x-ray Hartmann wavefront sensor, Opt. Lett. 31 (2006) 199–201.

[57] P. Mercère, et al., Wavefront closed-loop correction for x-ray microfocusing active optics, AIP Conf. Proc. 879 (2007) 722–725.

[58] C.M. Kewish, et al., Wave-optical simulation of hard x-ray nanofocusing by precisely figured elliptical mirrors, Appl. Opt. 46 (2007) 2010–2021.

[59] C.M. Kewish, et al., Reconstruction of an astigmatic hard x-ray beam and alignment of K-B mirrors from ptychographic coherent diffraction data, Opt. Express 18 (2010) 23420–23427.

[60] D. Spiga, X-ray beam-shaping via deformable mirrors: surface profile and point spread function computation for Gaussian beams using physical optics, J. Synchr. Rad. 25 (2018) 123–130.

[61] T. Weitkamp, B. Nöhammer, A. Diaz, C. David, E. Ziegler, X-ray wavefront analysis and optics characterization with a grating interferometer, Appl. Phys. Lett. 86 (2005) 054101.

[62] C. David, S. Rutishauser, M. Sprung, I. Zanette, T. Weitkamp, X-ray grating interferometry —Applications in metrology and wave front sensing, AIP Conf. Proc. 1466 (2012) 23.

[63] H. Wang, K.J.S. Sawhney, S. Bérujon, E. Ziegler, S. Rutishauser, C. David, X-ray wavefront characterization using a rotating shearing interferometer technique, Opt. Express 19 (2011) 16550–16559.

[64] S. Marathe, X. Shi, A. Khounsary, M.J. Wojcik, N.G. Kujala, A.T. Macrander, L. Assoufid, Development of single grating X-ray Talbot interferometer as a feedback loop sensor element of an adaptive X-ray mirror system, Proc. SPIE 9208 (2014) 92080D.

[65] B. Flöter, P. Juranic, S. Kapitzki, B. Keitel, K. Mann, E. Plönjes, B. Schäfer, K. Tiedtke, EUV Hartmann sensor for wavefront measurements at the Free-electron LASer in Hamburg, New J. Phys. 12 (2010) 083015.

[66] L. Raimondi, et al., Status of the K-B bendable optics at FERMI@Elettra FEL, Proc. SPIE 9208 (2016) 920804/1-11.

[67] M. Zangrando, D. Cocco, C. Fava, S. Gerusina, R. Gobessi, N. Mahne, E. Mazzucco, L. Raimondi, L. Rumiz C. Svetina, Recent results of PADReS, the Photon Analysis Delivery and REduction System, from the FERMI FEL commissioning and user operations, J. Synchr. Rad. 22 (2015) 565–570.

[68] F. Capotondi, E. Pedersoli, F. Bencivenga, M. Manfredda, N. Mahne, L. Raimondi, C. Svetina, M. Zangrando, A. Demidovich, I. Nikolov, M. Danailov, C. Masciovecchio, M. Kiskinova, Multipurpose end-station for coherent diffraction imaging and scattering at FERMI@Elettra free-electron laser facility, J. Synchr. Rad. 22 (2015) 544–552.

[69] C. Svetina, et al., The Low Density Matter (LDM) beamline at FERMI: optical layout and first commissioning, J. Synchr. Rad. 22 (2015) 538–543.

[70] P. Kirkpatrick, A.V. Baez, Formation of optical images by X-rays, J. Opt. Soc. Amer. 38 (1948) 766.

[71] H. Mimura, et al., Hard x-ray diffraction-limited nanofocusing with Kirkpatrick-Baez mirrors, Japan. J. Appl. Phys. 44 (2005) L539–L542.

[72] H. Yumoto, et al., At-wavelength figure metrology of hard x-ray focusing mirrors, Rev. Sci. Instrum. 77 (2006) 063712.

[73] H. Mimura, et al., Efficient focusing of hard x-rays to 25 nm by a total reflection mirror, Appl. Phys. Lett. 90 (2007) 051903.

[74] H. Mimura, et al., Breaking the 10 nm barrier in hard-x-ray focusing, Nat. Phys. 6 (2010) 122–125.

[75] K. Yamauchi, et al., Single-nanometer focusing of hard x-rays by Kirkpatrick-Baez mirrors, J. Phys. Condens. Matter. 23 (2011) 394206.

[76] R. Signorato, O. Hignette, J. Goulon, Multi-segmented piezoelectric mirrors as active/adaptive optics components, J. Synchr. Rad. 5 (1998) 797–800.

[77] L.A. Poyneer, T. McCarville, T. Pardini, D. Palmer, A. Brooks, M.J. Pivovaroff, B. Macintosh, Sub-nanometer flattening of 45 cm long, 45 actuator x-ray deformable mirror, Appl. Opt. 53 (2014) 3404–3414.

[78] R. Signorato, V.A. Solé, C. Gauthier, Performance of the ESRF ID26 beamline reflective optics, J. Synchr. Rad. 6 (1999) 176–178.

[79] D. Cocco, G. Bortoletto, R. Sergo, G. Sostero, I. Cudin, An hybrid active optical system for wavefront preservation and variable focal distance, Nucl. Instrum. Methods Phys. Res. A 616 (2010) 128–133.

[80] L. Raimondi, C. Svetina, N. Mahne, D. Cocco, A. Abrami, M. De Marco, C. Fava, S. Gerusina, R. Gobessi, F. Capotondi, E. Pedersoli, M. Kiskinova, P. Zeitoun, G. Dovillaire, G. Lambert, W. Boutu, H. Merdji, A.I. Gonzalez, D. Gauthier, M. Zangrando, Microfocusing of the FERMI@Elettra FEL beam with a K-B active optics system: spot size predictions by application of the WISE code, Nucl. Instrum. Methods Phys. Res. A 710 (2013) 131–138.